Research Article
doi.org/10.1002/ansa.202100062
Chemistry Europe
European Chemical Societies Publishing

Received: 25 November 2021
Revised: 16 March 2022
Accepted: 16 March 2022

TiO_2/CdS composite photocathode improves the performance and degradation of wastewater in microbial fuel cells

Jingying Ma[1] | Zhihao An[2] | Wenwen Zhang[3] | Jia Shen[1] | Yulin Qi[1] | Donghui Chen[2]

[1]Institute of Surface-Earth System Science, School of Earth System Science, Tianjin University, Tianjin, China

[2]School of Chemical and Environmental Engineering, Shanghai Institute of Technology, Shanghai, China

[3]School of Environmental Science and Engineering, Donghua University, Shanghai, China

Correspondence
Yulin Qi, Institute of Surface-Earth System Science, School of Earth System Science, Building No.16, Tianjin University, 92 Weijin Road, Nankai District, Tianjin, China.
Email: yulin.qi@tju.edu.cn
Donghui Chen, School of Chemical and Environmental Engineering, Shanghai Institute of Technology, 100 Haiquan Road, Fenxian District, Shanghai, China.
Email: chendhisit@163.com

Funding information
Shanghai Institute of Technology, Grant/Award Numbers: DCX2019198, 50578020; National Natural Science Foundation of China, Grant/Award Number: 42007290

Abstract

Optimization of dye decolourization for wastewater and power production are explored in dual-chamber microbial fuel cells (MFCs) with TiO_2/CdS photocathodes. The rapid reduction of azo dye methylene blue (MB) and power production were enhanced with TiO_2/CdS photocathode under illumination. The analysis of electrochemical impedance spectra indicated that the photocatalysis of TiO_2/CdS accelerated the electron transfer process of photoelectrode reduction. Moreover, the UV-visible light spectrophotometer showed that the maximum degradation of the MFCs was 98.25%, which illustrated that MB may be cleaved by photoelectrons generated by light irradiation on the illuminated TiO_2/CdS photocathode. Finally, the power production of MFCs in this work promoted reductive decolourization of the dye MB solution.

KEYWORDS
bio-electrochemical, photoelectrode, photoreduction, TiO_2/CdS

1 | INTRODUCTION

In recent years, the production and use of printing and dyeing have been rapidly developed, resulting in a large amount of dye wastewater containing organic dyes.[1–3] It is well known that dye wastewater can seriously affect the local ecological environment, especially the healthy growth of aquatic organisms due to its wide variety, high concentration, complex organic components, poor bioavailability, strong toxicity and emissions.[4] Therefore, developing a low cost, high efficiency and reliable dye wastewater treatment technology has been particularly important for industrial dye wastewater degradation.[5–7]

Recently, the photoelectric coordinated system for wastewater treatment has attracted more and more attention.[8,9] The microbial fuel cell with photoelectrodes, as a new technology with biological power generation and wastewater treatment, provides a promising option for the treatment of dye wastewater.[10–12] In the microbial fuel cells (MFCs) with photoelectrodes, organic substances (such as acetate) are oxidized by the electricity-generating microorganisms in the anode chamber. The electrons released to the anode are transferred to the cathode by the external circuit and then combine with an electron acceptor to form water.[13–17] Meanwhile, the process in which photo-generated holes are left as electron acceptors and combined with electrons transferred from the anode increases the reaction rate of the cathode.[18] Photoelectrodes have an important impact on the capacity and degradation of MFCs, and therefore many researchers have focused on developing efficient photoelectrodes.[19,20] Li et al.[21]

Research Article
doi.org/10.1002/ansa.202100062
Chemistry Europe
European Chemical Societies Publishing

prepared photocatalytic electrodes by coating polydopamine and horseradish peroxidase on titanium dioxide (TiO_2) nanotube arrays and exhibited good sensitivity and selectivity for hydrogen peroxide biosensing. Chen et al.[22] designed a new type of microbial fuel cell with a nano-structured TiO_2 semiconductor photocathode. Its proton exchange membrane can separate the anode and cathode compartments, thereby overcoming the thermodynamic barriers of producing hydrogen from acetic acid without the help of a power source. Lu et al.[11] introduced rutile coated cathode in MFCs, which can achieve maximum power density and improve conversion efficiency under light irradiation. However, TiO_2 can only perform photocatalysis under UV irradiation, and the wide band gap seriously hinders its wide application.[23] On the one hand, the photocatalytic reaction of electrodes is considered as a surface reaction, and the specific surface area of nanostructured catalysts affects the catalytic efficiency. On the other hand, the specific surface area of untreated TiO_2 materials is limited, and most of them cannot directly participate in the photocatalysis process. However, the composite of other narrow band gap semiconductor materials and TiO_2 can solve the above problems, and further improve the photocatalytic performance. It has huge application potential in the application of photocatalytic wastewater treatment due to low photogenerated electron-hole pair separation efficiency, carrier recombination ultrafast and cadmium sulfide (CdS) extremely aggregated nanoparticles.[24]

Therefore, this work mainly prepared CdS-doped photocathodes to study the electrode's performance in generating electricity and degrading methylene blue (MB) in MFCs. In order to explore the performance of photocathode and CdS, several test methods were used. First, the surface morphology of the synthesized photocathode was characterized by a scanning electron microscope (SEM) and energy dispersive spectrometer (EDS). X-ray photoelectron spectroscopy (XPS) and X-ray diffraction analysis (XRD) were used for characterization in order to observe the morphology and crystal structure of the electrode. Second, the photoelectrochemical method was used to detect the influence of light on the electrochemical activity of the photocathode MFC in MB. Finally, a UV-visible light spectrometer (UV-vis) was used to study the dye degradation ability of MFC. This work further revealed the potential possibility of TiO_2/CdS with the photocatalytic activity on improving composite for photocatalytic degradation of dye wastewater in MFCs and provided a novel idea for the enhancing utilization of photocatalysts. We hope that this research could contribute to the MFCs in wastewater treatment and their development in the future.

2 | MATERIALS AND METHODS

2.1 | MFCs construction and operation

We used a typical two-chamber microbial fuel cell reactor. The anode chamber and the cathode chamber consisted of two equal volume lysoglass chambers (Wenoote, Shanghai, China). consisted of a valid volume of 100 ml, separated by a cation exchange membrane (Qianqiu, Zhejiang, China). The anode chamber was sealed with rubber plugs to maintain an oxygen-deprived or anaerobic environment, the cathode chamber had a small hole of 10 mm, and the continuous injection of oxygen using an air pump had provided sufficient oxygen for electrochemical reactions. The external connection was 20 Ω resistance, which was connected by titanium wire between the anode and cathode at intervals of 10 cm. Install a visible light source (Antoine) 10 cm outside the reactor; Change Lighting Technology Co., Ltd., Dongguan, China) to observe the effects of light on microbial fuel cell capacity and degradation. Anode electrolyte by mineral salt (1.98 g L^{-1}), NH_4Cl (0.31 g L^{-1}), K_2HPO_4 (6.59 g L^{-1}), KH_2PO_4 (2.88 g L^{-1}), $C_6H_{12}O_6$ (1.00 g L^{-1}) and CH_3COONa (1.42 g L^{-1}) composition. Cathode electrolyte by $NaNO_3$ (1.40 g L^{-1}), $NaHCO_3$ (0. 98 g L^{-1}), KCl (0.11 g L^{-1}) and MMD (MB, 10 mg L^{-1}) composition.[25] Microbes in the anode chamber were inoculated from MFCs that have been in operation for 3 years, initially from wetland sediments. All reactors operated throughout the day in a 25 ± 2°C hydrothermal culture tank (GHP-9080; Bluepard, shanghai, China).

2.2 | Preparation of CdS photoelectrode

TiO_2/CdS photoelectrodes were prepared by anode oxidation and electro-deposition on titanium plates (3.0 × 2.0 × 0.1 cm, purity 99%). The specific experimental steps were as follows: First, the titanium plate was immersed in 15 wt% sodium hydroxide solution, heated to 60°C, the constant temperature lasts 30 min, after cooling with deionized water cleaning three times; Place the pre-treated titanium plate parallel to the graphite plate (2 cm) in an electrolytic cell, using 5 wt% NH_4F, 20vt%H_2O and 80 wt% ethylene glycol solution, and the anode oxidation was carried out at 2 h and then calcined at 450°C in the Mafu furnace 2 h. The electrode was immersed in a mixed solution of 0.1M$CdCl_2$ and 0.1MNaS_2O_3, graphite was used as the counter electrode, 1.1 V cathode current was applied for 1 h, and then placed in a muffle furnace (SX2-0.5-10A; Shaoxing, China) for annealing at 150°C for 30 min.

2.3 | Electrode characterizations

The surface features of the prepared electrode were first determined using an SEM (JSM-5600 LV, Tokyo, Japan) and the surface composition elements of the electrode were detected by the commonly configured EDS (20.0 kV). The composition of the surface elements of the electrode was analyzed by XPS. The crystal structure of the prepared electrodes was analyzed by X-ray diffraction technology (XRD, Rigaku D/MAX-2550VBþ/PC; Tokyo, Japan).

2.4 | Photo-electrochemical experiments

In this study, the output voltage of the microbial fuel cell was recorded by the data test acquisition system (BT-2016C; Lanbts, Wuhan, China) every 30 seconds. When the maximum production capacity was reached, the electrochemical workstation (CHI760E; Chenhua, Shanghai, China) was used to evaluate the electrochemical characteristics

Research Article
doi.org/10.1002/ansa.202100062
Chemistry Europe
European Chemical Societies Publishing

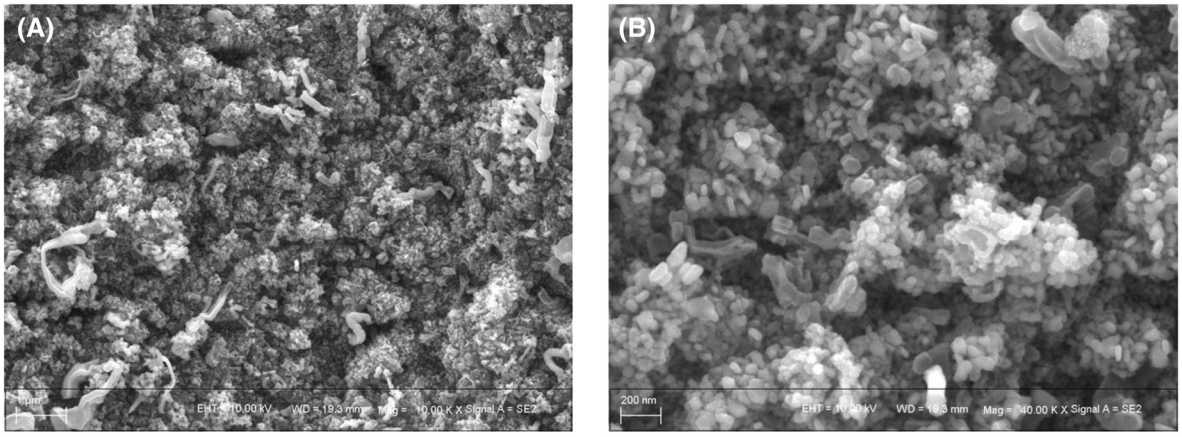

FIGURE 1 Scanning electron microscope (SEM) micrograph of (A) TiO_2/CdS electrode (10 K). (B) TiO_2/CdS electrode (40 K)

of the MFCs photocathode, including linear sweep voltammetry (LSV), cyclic voltammetry (CV), and electrochemical impedance spectroscopy (EIS), Tafel curve and transient photocurrent response. Electrochemical research was mainly carried out in a three-electrode system, in which TiO_2/CdS, Ag/AgCl (sat. KCl) and graphite electrodes were used as working electrode, reference electrode and counter electrode, respectively. Perform a linear sweep volt-ampere (LSV) curve from 0.5 V to -0.5 V at a sweep rate of 0.2 mV s-1 in the electrolyte. Electrical impedance spectroscopy measured the electrode resistance in the range of 10 Hz–500 kHz and used the software Z-SimpWin to fit the calculated data with a suitable model. The Tafel curve was measured at a scanning rate of 1 mV s-1 in the overpotential range of 0.5 to -0.5V to evaluate the corrosion resistance of the photocathode. The light source used in the transient photocurrent response curve was a Xe lamp, and the interval between each turn on and off was 20 s. The light absorption performance of the photocathode was analyzed by UV-vis diffuse reflectance spectroscopy to obtain the forbidden bandwidth of the photocathode.

When the output voltage of the startup reactor reached a stable value, 100 ml of MB solution was injected into the cathode chamber, and water samples in the cathode chamber were taken every 30 min. The degradation degree of MB dye was measured by a UV spectrophotometer, and the absorption wavelength of the dye solution was determined to be 664 nm. The following formula was performed to calculate the degradation amount of MB:

$$q_t = \frac{(C_t - C_0)}{C_0} \quad (1)$$

where C_0(mg L^{-1})is the initial dye concentration, C_t(mg L^{-1})is the dye concentration at equilibrium.

3 | RESULTS AND DISCUSSION

3.1 | Characterization of the photocathode

The microscopic surface morphology and structure of the electrode were characterized by SEM.[4] It could be seen that Figure 1A,B show SEM images of TiO_2/CdS electrodes with high magnification, which mean that after anodization, the smooth surface of the titanium plate becomes a rough surface, and CdS nanometers were electrodeposited in situ on the TiO_2 electrode. After the particles, the surface of the electrode was overlapped and wrapped by a large number of CdS quantum dot nanoparticles, which enhanced the light utilization performance and the electron transfer rate. To this end, an energy spectrum SEM-EDS was also carried out to verify the distribution of CdS on the electrode surface. As shown in Figure 2B,C, TiO_2 was uniformly distributed on the electrode surface. As shown in Figure 2D,E, the CdS quantum dots were widely distributed on the electrode surface, obviously more than titanium and oxygen. This showed that CdS is successfully synthesized on the surface of the electrode, which could provide more quantum dots.

In order to study the chemical state and surface composition of the electrode, we used XPS to study the XPS characteristics of the TiO_2/CdS electrode. The standard binding energy of C_{1S} of 284.6 eV was used to correct the binding energy positions of all peaks in Figure 3. As shown in Figure 3A, in the survey spectrum of the electrode, the characteristic peaks of the three elements were detected, corresponding to the three elements Ti, S and Cd. The peak of C1s came from the XPS test instrument itself. In Figure 3B, the Ti_{2p} peak is higher in the range of 450–475 eV. The double peaks at 458.3 and 464.5 eV correspond to $Ti^{4+}2p^{2/3}$ and $Ti^{4+}2p^{1/2}$, respectively, which were mainly $Ti^{4+}(TiO_2)$. In Figure 3C,D are the XPS spectra of CdS. The band intensities of Cd_3d_3, Cd_3d_5 and S_{2p} were 411.89, 405.17, 161.47, and 162.59 eV, respectively, which also correspond to the Cd^{2+} and S^{2-} ions in CdS. Among them, the presence of a weak peak at 168.52 eV indicated that S^{2-} was slightly oxidized to SO_4^{2-}. The results further indicated that TiO_2 and CdS were completely present in the electrode.

In order to study the crystal phase of the prepared electrode, we used XRD to analyze the crystal structure of the electrode material. As shown in Figure 4, the peaks observed at 25.331°, 35.174°, 38.516°, 40.239°, 48.093°, 53.096°, 53.875°, 54.962°, and 70.691° correspond to TiO_2. Two distinct reflections of anatase TiO_2 appeared at 25.331°, 38.516°, 53.875°, 54.962°, 70.691°, and 48.093°, which corresponded to (101, (112), (105), (211), (220) And (200) crystal plane (PDF#21-1272). Others were at 35.174°, 40.239°, 53.096°, corresponding to the

Research Article
doi.org/10.1002/ansa.202100062
Chemistry Europe
European Chemical Societies Publishing

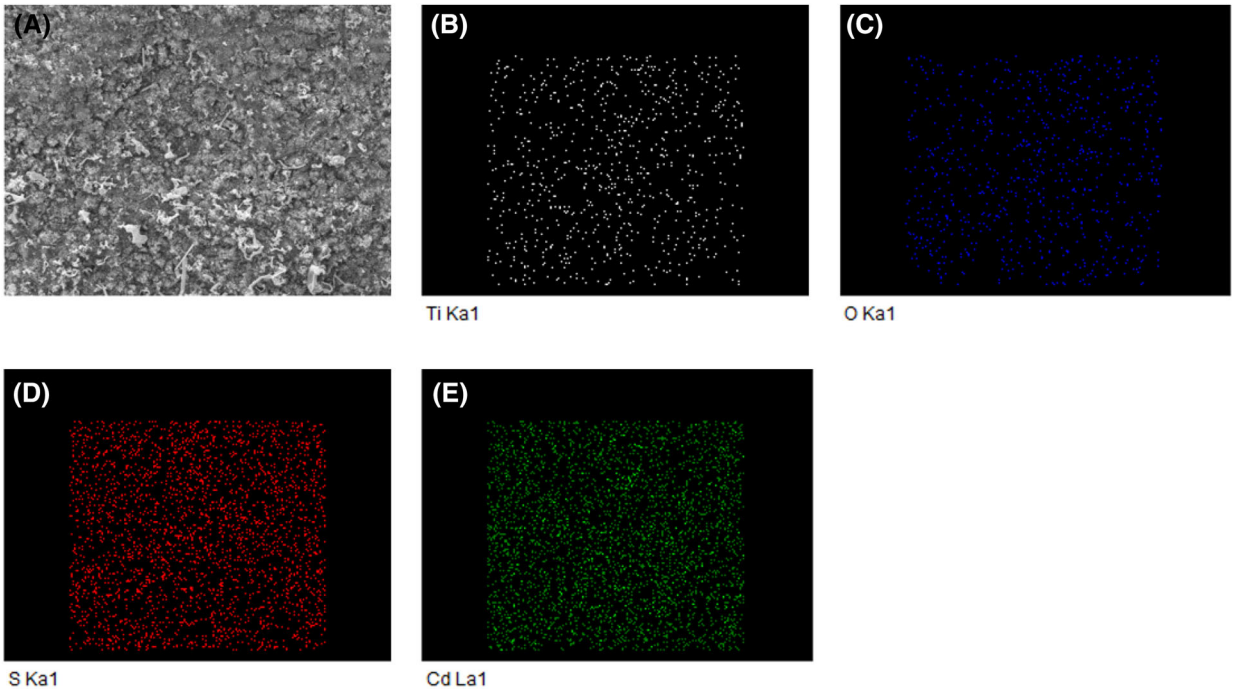

FIGURE 2 (A) Scanning electron microscope (SEM) image of the TiO_2/CdS electrode. (B–E) Elemental maps of as-prepared electrode

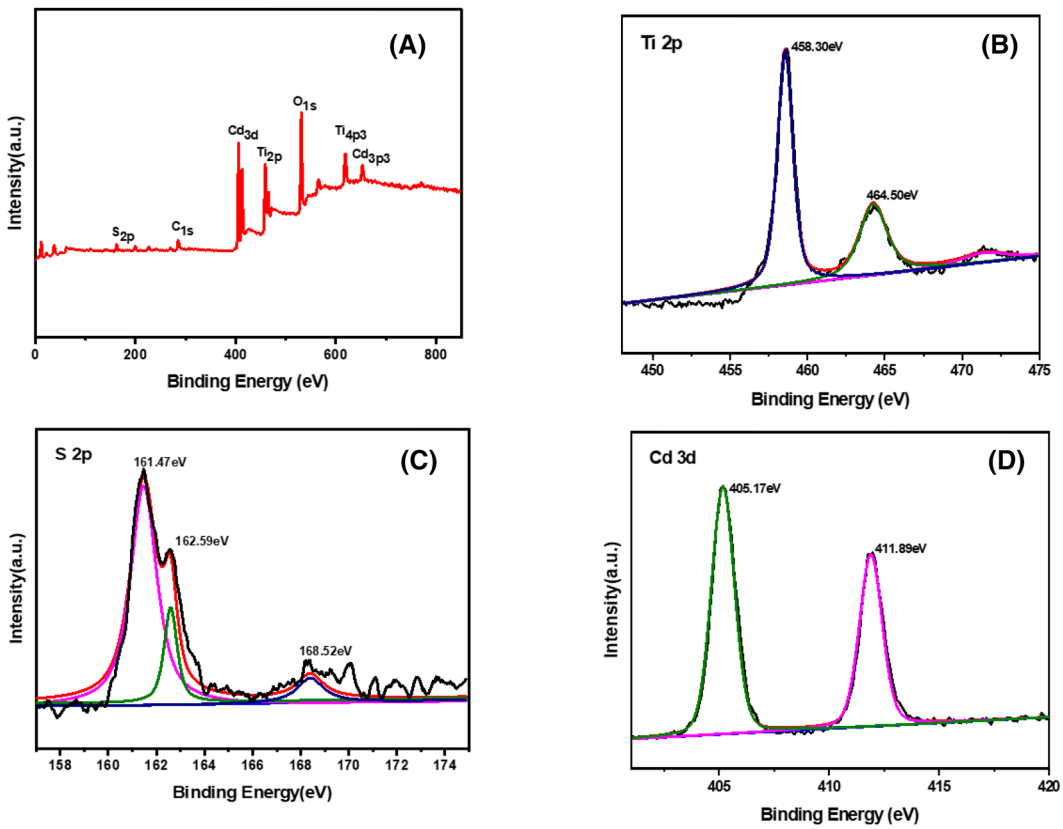

FIGURE 3 (A) X-ray photoelectron spectroscopy (XPS) survey spectra CdS electrode. (B) High-resolution Ti 2p XPS spectra of CdS electrode. (C) High-resolution S 2p XPS spectra of CdS electrode. (D) High-resolution Cd 3d XPS spectra of CdS electrode

Research Article
doi.org/10.1002/ansa.202100062
Chemistry Europe
European Chemical Societies Publishing

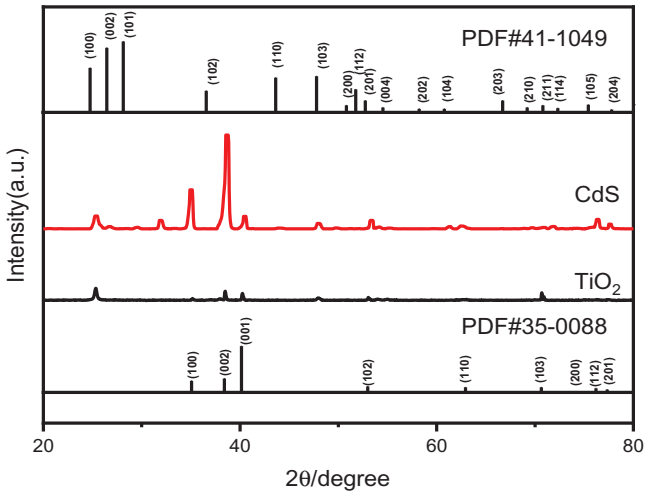

FIGURE 4 X-ray diffraction (XRD) pattern of different electrodes

(101), (200) and (211) crystal planes of rutile TiO_2. According to the hexagonal wurtzite structure Greenockite CdS standard card, the peak values of 26.803 and 69.707 corresponded to (002)s and (210) crystal planes, respectively. According to the cubic CdS standard card, 31.948 and 71.883 corresponded to the (200) and (331) crystal planes, respectively, which verified the cubic morphology of CdS in Figure 1B of the SEM. The size of the crystal grain size was calculated according to the Scherer formula:

$$D = 0.9\lambda / (\beta cos\theta) \quad (2)$$

In the formula, λ is 0.154 nm, which is the wavelength of the CuKα line. β is the half-width corresponding to a peak with a certain radian, and θ is the Bragg angle. From this calculation, the crystal grain sizes of TiO_2 and CdS were 62.543 and 42.24 nm, respectively. According to related literature, this increase in specific surface area by reducing the size of the crystal size was beneficial to promote the Photoelectrocatalytic (PEC) reaction process.

3.2 | Electrochemical characterization of photoelectrodes

The peak height and symmetry of the oxidation wave and the reduction wave obtained from the CV could be used to judge the reversibility of the reaction of the electroactive material on the electrode surface.[26] As shown in Figure 5A, the heights of the oxidation wave and the reduction wave of CdS and TiO_2 were different, the symmetry of the curve was poor, which showed that the reaction of the two electrodes is irreversible. Compared to TiO_2, CdS had an obvious oxidation peak current, which promoted the electrochemical reaction activity. As shown in Figure 5B, under light conditions, the redox peak of CdS was significantly higher than the height under dark conditions, resulting in different electrochemical activities of the electrode. The CV curve showed that the CdS electrode has higher electrochemical reaction activity under light conditions, which was beneficial to speed up the electron transfer rate of the MFCs reactor.

In order to further determine the electrochemical parameters of the anode, an EIS experiment was carried out.[27] Figure 6A,B is the measured Nyquist diagram of the electrode obtained under different conditions. As shown in Figure 7A, the fitted equivalent circuit under dark conditions was $R_1(CPE_1R_2)O$, R_1 represents the ohmic resistance of the electrolyte, CPE_1 represents the electric double-layer capacitance, and R_2 represents the charge transfer resistance, which reflected the intensity of the redox reaction. O stands for finite Warburg. The fitted equivalent circuit under CdS illumination was $R_1(CPE_1R_2)$ $(CPE_2R_3)O$, CPE_2 and R_3 represents the oxide film electrical impedance and the oxide film capacitor, respectively (Figure 7B). Under the light, the charge transfer resistance of TiO_2 in the control group was 7.673×1014 Ω, and the minimum charge transfer resistance of CdS was 1509 Ω. The charge transfer resistance was determined by the electrode reaction kinetics. The smaller the value, the faster the electron transfer process on the electrode. The data fitting results of the Z-SimpWin software showed that the charge transfer resistance of the CdS electrode under light conditions is the smallest (Table 1). The reason may be that it provides more electrochemically active sites and high electron transfer during light irradiation.

The Tafel curve test was to change the electrode potential as a function of its own variable in a certain linear relationship during the whole process and measured the tracking of the electrode potential change by the current flowing through the electrode. The higher the corrosion potential of the electrode, the slower the corrosion rate, and the corrosion rate was related to the phenomenon of metal polarization. The higher the self-corrosion current density, the faster the corrosion rate and the worse the corrosion resistance. Figure 6C was the Tafel curve of different electrodes. The electrochemical corrosion parameters were calculated in Table 2, and the results showed that the corrosion potential of CdS is the lowest and the corrosion resistance is the best, which provided a good foundation for the long-term operation of MFCs.

The LSV curve showed that CdS has superior ORR catalytic activity under the light. It could be seen the CdS electrode under light has a smaller overpotential, a large current density, and the best catalytic performance compared to dark conditions (Figure 6D). The main reason may be that more electrochemically active sites and higher conductivity are exposed, which greatly increased the possibility of the prepared electrode being in contact with electrons, thereby further speeding up the ORR process. At the same potential, the current density and the catalytic performance of the electrode exhibited a proportional relationship.

3.3 | The optical absorption characteristics of electrodes

Figure 8 shows the UV-vis diffuse reflectance absorption spectrum of the electrode. It could be seen that nano-TiO_2 has a strong absorption peak at 200–380 nm in the UV region, while the CdS-doped composite electrode had strong absorption at 200–800 nm in the UV and

Research Article
doi.org/10.1002/ansa.202100062
Chemistry Europe
European Chemical Societies Publishing

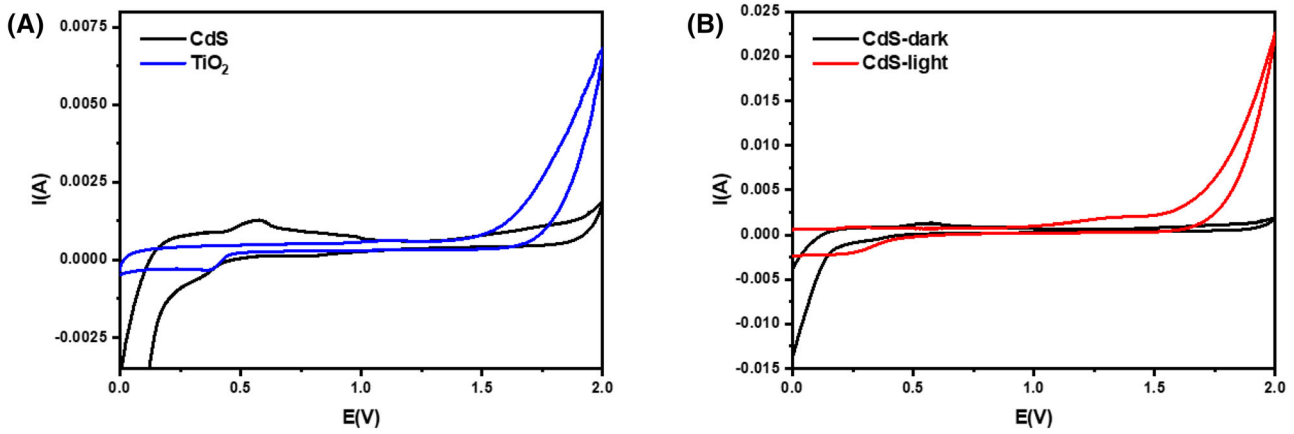

FIGURE 5 (A) Cyclic voltammetry (CV) curves of TiO_2 and CdS electrode electrolyte in three-electrode mode. (B) CV curve of CdS electrode in the dark and light

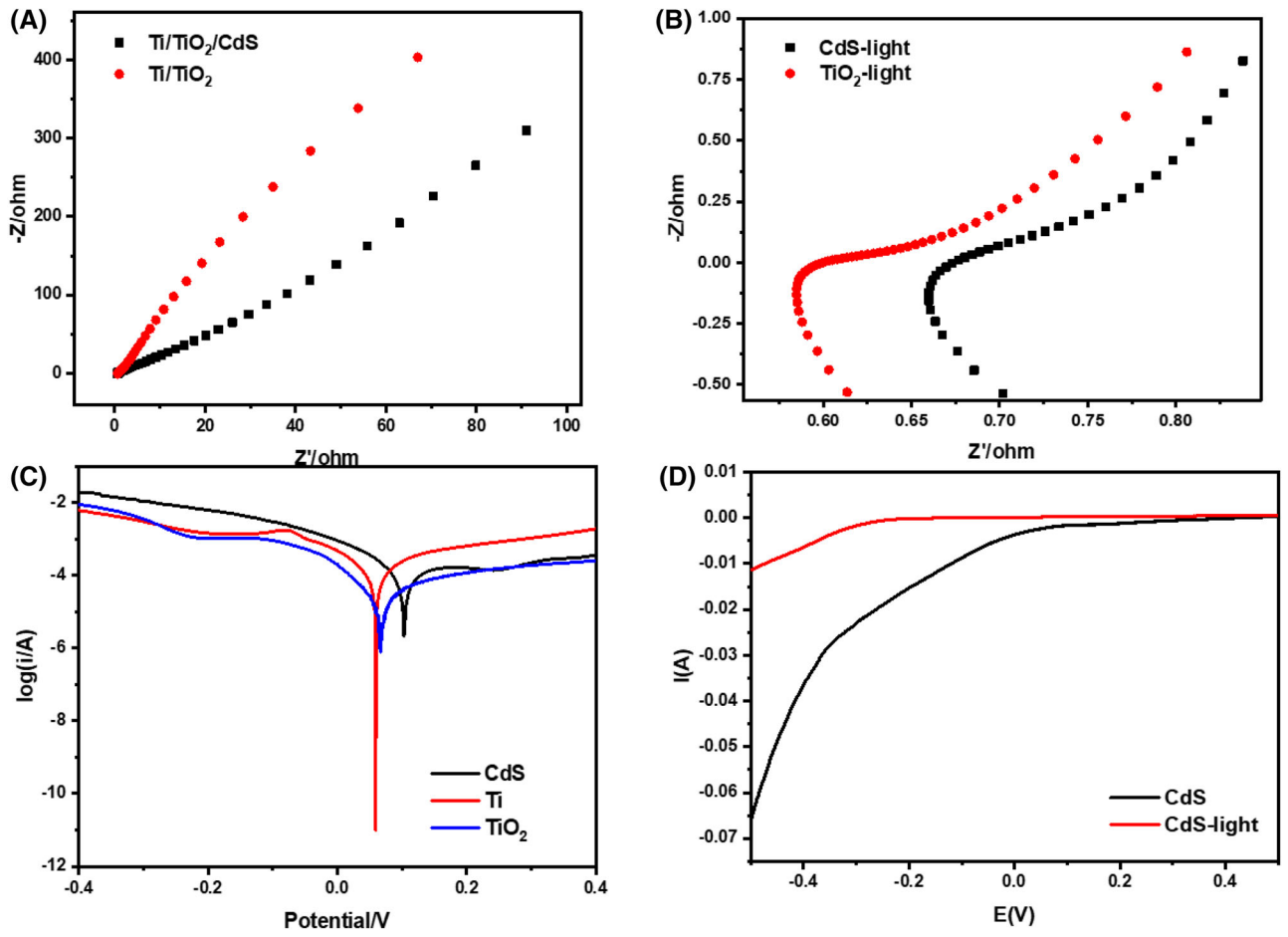

FIGURE 6 (A) Nyquist plots of different electrodes. (B) Nyquist plots of CdS electrode in the dark and light. (C) Tafel polarization curves of different electrodes. (D) Linear sweep voltammetry (LSV) curves of CdS under dark and light conditions

TABLE 1 The fitting results of different cathodes electrodes from Nyquist plots

			(A) Dark conditions		(B) Under illumination	
Cathodes	R_2 (Ω cm^{-2})	CPE (Ω $cm^{-2}S^n$)	R_2 (Ω cm^{-2})	CPE (Ω $cm^{-2}S^n$)	R_3 (Ω cm^{-2})	CPE (Ω $cm^{-2}S^n$)
TiO_2	1.027×10^{4}	1.209×10^{-4}	3.062×10^{13}	4.936×10^{-4}	7.673×10^{14}	3.211×10^{-2}
CdS	1.745×10^{-2}	4.435×10^{-14}	1.02×10^{4}	9.994×10^{-5}	1.509×10^{3}	2.14×10^{-3}

Research Article
doi.org/10.1002/ansa.202100062
Chemistry Europe
European Chemical Societies Publishing

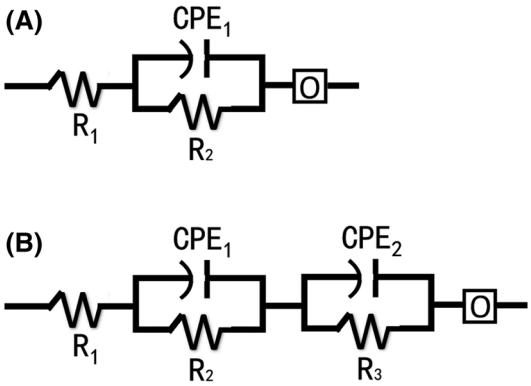

FIGURE 7 Equivalent circuit models were used in the analysis of electrodes in microbial fuel cells (MFCs). (A) Under the dark conditions. (B) Under illumination

TABLE 2 Corrosion parameters of different electrodes

	Ecorr (vs. SCE) (V)	Icorr (μA cm^{-2})
Ti	0.059	11.69
TiO_2	0.067	7.175
CdS	0.103	5.725

visible regions (Figure 8a). The absorption of the CdS-doped composite electrode in the visible light region was higher than that of the TiO_2 electrode, which was caused by the electron transfer on the conjugated compound produced by polymer recombination. Electrons flowed from substances with a higher conduction band (CB) energy level to TiO_2 with a lower CB energy level, facilitating photogenerated carrier separation.[28] CdS could effectively extend the absorbance range of TiO_2 to the visible region.[29] The electrons could migrate to TiO_2 more effectively, and the cavities were oxidized and consumed by transfer, which reduced the recombination of carriers and enhanced the photocatalytic activity.[30] According to Equation (2), the forbidden bandwidth of the electrode material was estimated, and the calculation results were shown in Figure 8 b and c.

$$(\alpha hv) = \beta(hv - Eg)^{m/2} \quad (3)$$

Among them, α is the absorption coefficient, β is the proportional constant related to the band tailing parameter, hv is the incident photon energy related to the Planck constant, and Eg is the indirect optical energy gap. The energy (hv) and (αhv) 2 could be used as the x and Y coordinate axes to draw the band gap diagram of TiO_2 and CdS doped electrodes. The arctangent was made along the intersection of the calculated curve and the x-axis, and the value obtained at the intersection was the band gap value of the TiO_2 and CdS-doped electrode. Compared to the TiO_2 electrode, the absorption of CdS for light was significantly enhanced, and the range of absorption was expanded. According to Figure b,c, the band gap of TiO_2 was about 3.22 eV and the band gap of the TiO_2/CdS composite electrode was about 3.16 eV. The positions of the valence band (VB) and the CB of CdS and TiO_2 can be calculated by empirical equations,[30,31] the CB positions are -0.48 eV and−0.30 eV and the VB positions are 1.86 and 2.92 eV, respectively. Based on the results above, there are differences in the band gap between CdS and TiO_2, resulting in band overlap. This structure leads to the transfer and separation of photogenerated carriers between catalysts of different energy levels, which effectively suppresses photogenerated electron-hole recombination, improves the photogenerated electron yield and catalytic efficiency of TiO_2, and effectively expands the light response range.

3.4 | The degradation performance of photoelectrodes

The instantaneous photocurrent response curve of the prepared photoelectrode under visible light irradiation was shown in Figure 9. The curve showed that the photocurrent response of the CdS electrode is

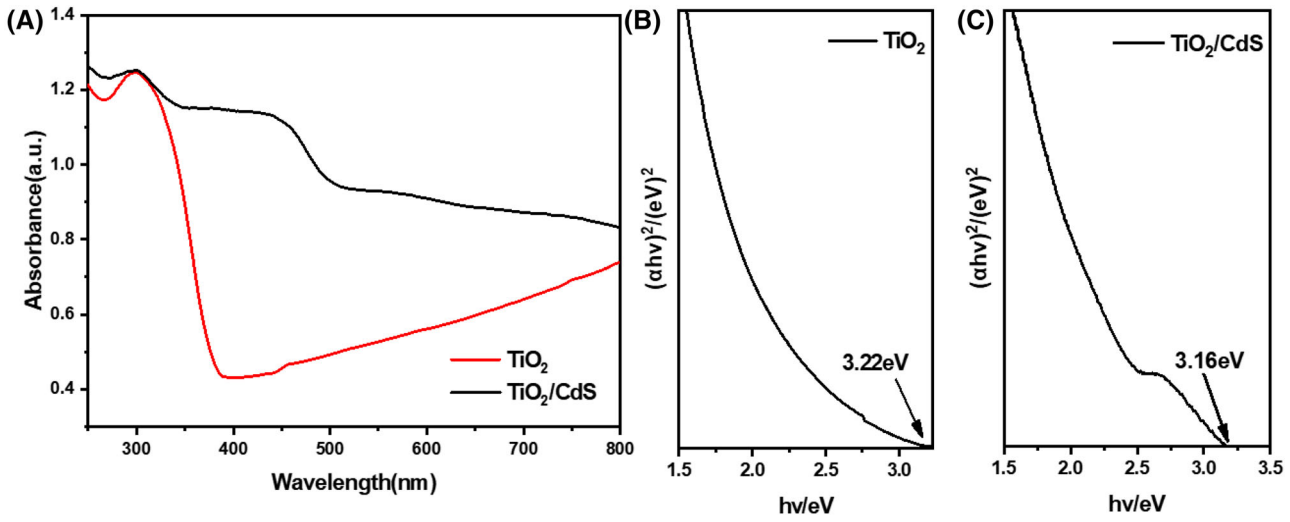

FIGURE 8 (A) UV-Visible light absorption diffuse reflectance spectroscopy (DRS) patterns. (B) Calculated energy band gap of TiO_2. (C) calculated energy bandgap of TiO_2/CdS

Research Article
doi.org/10.1002/ansa.202100062
Chemistry Europe
European Chemical Societies Publishing

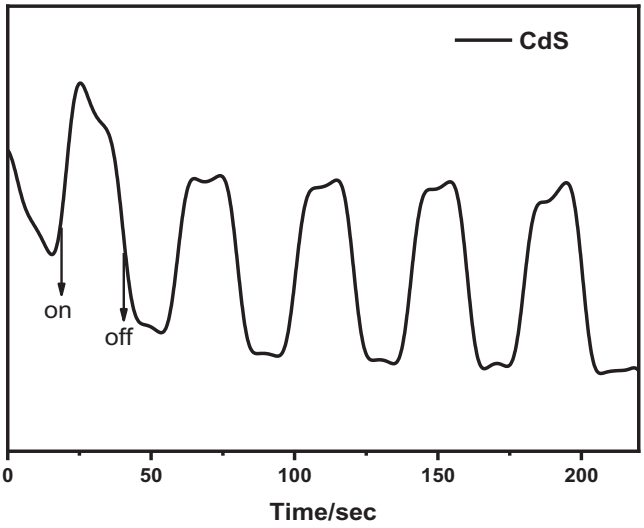

FIGURE 9 Transient photocurrent responses of microbial fuel cells (MFCs) with CdS photocathode

obvious, and the test time interval between the change of light and dark conditions is 20 s. Generally, the separation ability of electron and hole pairs was proportional to the photocurrent density, which had a significant effect on improving photocatalytic activity. It could be seen from the response curve that the photocurrent response intensity of the photoelectrode is relatively strong, possibly due to the doping of CdS, which had a positive effect on the separation/transport of electrons and holes, and further improved the production capacity of MFCs.

In order to study the degradation performance of the photoelectrode of the microbial fuel cell to the dye, we used a UV-vis spectrophotometer to evaluate the MB solution. Under visible light irradiation, 100 ml of 10 mg/L MB solution was added to the MFC with a CdS photocathode. The result of the spectral scan was shown in Figure 10A. The intensity of the characteristic peak at 663 nm gradually decreased with time and disappears after 2 h. This showed that CdS photoelectrodes can effectively degrade MB in MFCs. Formula (1) was used to calculate the concentration of MB in MFC under different reaction conditions. Figure 10B showed that photocathodes under different conditions have different photocatalytic effects. The degradation curve showed that the closed-circuit MFC has the lowest degradation rate under dark conditions, and the open-circuit MFC has the highest degradation rate under light conditions. Among them, the degradation rates of open-circuit MFC under dark and light conditions reached 32.67% and 98.25%, respectively, and the degradation rates of closed-circuit MFC under dark and light conditions reached 0.20% and 79.86%, respectively. Under light conditions, the degradation rate of open circuit MFC was 18.69% higher than that of a closed circuit. Under dark conditions, the degradation rate of open circuit MFC was 32.47% higher than that of a closed circuit. It showed that the photoelectric synergy of MFCs can further promote the degradation of dyes.

4 | CONCLUSION

In this article, a photocathode doped with CdS was prepared, and the performance of the electrode in generating electricity and degrading MB in MFCs was studied. First, the surface morphology of the synthesized photocathode was characterized by SEM and EDS, and the results showed that CdS was uniformly distributed on the electrode surface. Second, CV showed that the CdS electrode has high electrochemical activity, which further improved the oxidation-reduction performance of the reactor. Electrical impedance spectroscopy showed that the CdS electrode has low ohmic impedance and high conductivity, which could increase the electron transfer rate. The LSV curve showed that the CdS electrode has high ORR activity. The diffuse reflectance spectrum showed that the CdS photocathode has extended the spectral response range and has a clear light response under visible light. The degradation

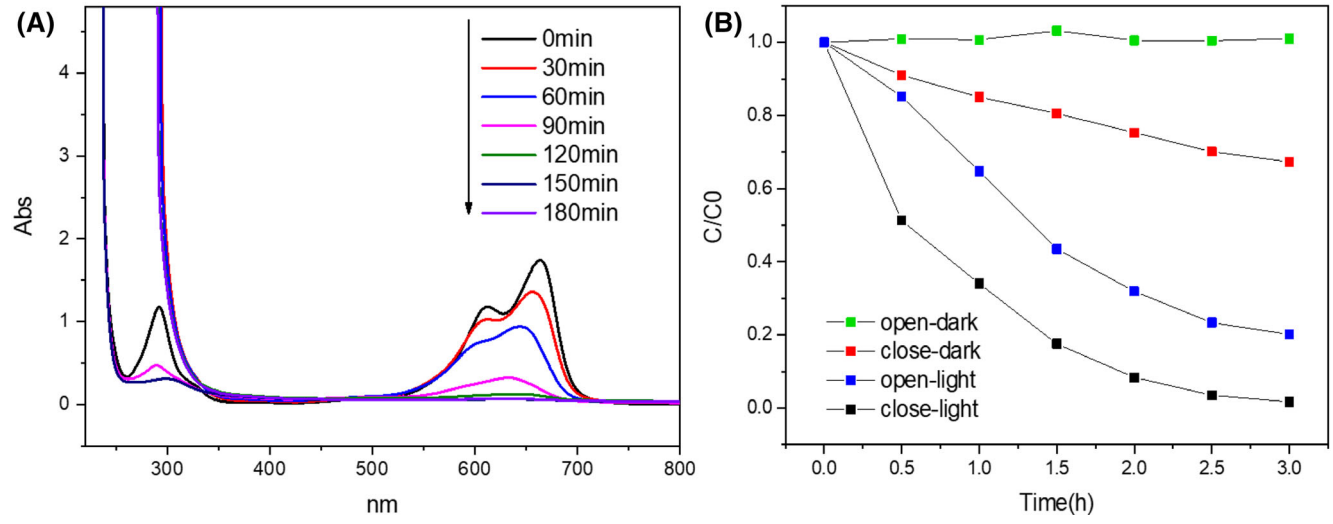

FIGURE 10 (A) Photo images of methylene blue (MB) in the photodegradation. (B) Degradation efficiency curve during open/closed circuit/light-dark conversion

experiment of MB solution showed that the best degradation condition is that the closed-circuit MFC is under light conditions. The reason for the high degradation rate of the composite material was that CdS broadens the electrode spectral response range, and the photogenerated electrons and the electrons transferred from the anode participate in the organic reduction. During the process, the bond breakage and decolourization of MB were realized. In short, photoelectric MFCs provide new ideas for the degradation of dye wastewater.

ACKNOWLEDGEMENTS

The authors would like to express appreciation for the Innovation Project of College Students Science and Technology provided by Shanghai Institute of Technology (no. DCX2019198), the University Funded Project of Shanghai (no. 50578020) and the funding by the National Natural Science Foundation of China (no. 42007290). Manhong Huang (Donghua University) were gratefully acknowledged to conduct the research work for the experimental guidance support.

CONFLICT OF INTEREST

There is no conflict of interest associated with this work. Yulin Qi serves on the editorial board of Analytical Science Advances.

AUTHOR CONTRIBUTIONS

The manuscript was written through the contributions of all authors.

DATA AVAILABILITY STATEMENT

The data that support the finding of this study are available from the corresponding author on reasonable request.

REFERENCES

1. Kong S, Zhang W, Gao S, Chen D. Immobilized CeO 2 for adsorption of azo dye. *J Exp Nanosci*. 2019;14:107-115.
2. Tavangar T, Jalali K, Alaei Shahmirzadi MA, Karimi M. Toward real textile wastewater treatment: membrane fouling control and effective fractionation of dyes/inorganic salts using a hybrid electrocoagulation nanofiltration process. *Sep Purif Technol*. 2019;216:115-125.
3. Zheng Y, Cheng B, Fan J, Yu J, Ho W. Review on nickel-based adsorption materials for Congo red. *J Hazard Mater*. 2020;403:123559.
4. Mousavi M, Soleimani M, Hamzehloo M, Badiei A, Ghasemi JB. Photocatalytic degradation of different pollutants by the novel gCN-NS/Black-TiO_2 heterojunction photocatalyst under visible light: Introducing a photodegradation model and optimization by response surface methodology (RSM) *Mater Chem Phys*. 2021;258:123912.
5. Han H-X, Shi C, Yuan L, Sheng G-P. Enhancement of methyl orange degradation and power generation in a photoelectrocatalytic microbial fuel cell. *Appl Energy*. 2017;204:382-389.
6. Kaushik A, Gola D, Raghav J, et al. Synthesis of Silver Nanoparticles using Egg White: Dye Degradation and Antimicrobial Potential. *Biointerface Res Appl Chem*. 2022;12:2361-2372.
7. Reghioua A, Barkat D, Jawad AH, Abdulhameed AS, Khan MR. Synthesis of Schiff's base magnetic crosslinked chitosan-glyoxal/ZnO/Fe3O4 nanoparticles for enhanced adsorption of organic dye: Modeling and mechanism study. *Sustain Chem Pharm*. 2021;20:15.
8. Antolini E. Photoelectrocatalytic fuel cells and photoelectrode microbial fuel cells for wastewater treatment and power generation. *J Environ Chem Eng*. 2019:7.
9. Liu J, Chen J, Wu Z, et al. Enhanced visible-light photocatalytic performances of ZnO through loading AgI and coupling piezo-photocatalysis. *J Alloys Comp*. 2021;852:156848.
10. Cai T, Meng L, Chen G, et al. Application of advanced anodes in microbial fuel cells for power generation: a review. *Chemosphere*. 2020;248:125985.
11. Lu A, Li Y, Jin S, et al. Microbial fuel cell equipped with a photocatalytic rutile-coated cathode. *Energy Fuels*. 2010;24:1184-1190.
12. Talooki EF, Ghorbani M, Rahimnejad M, Lashkenari MS. Evaluation of a visible light-responsive polyaniline nanofiber-cadmium sulfide quantum dots photocathode for simultaneous hexavalent chromium reduction and electricity generation in photo-microbial fuel cell. *J Electroanal Chem*. 2020;873:114469.
13. Cai T, Huang M, Huang Y, Zheng W. Enhanced performance of microbial fuel cells by electrospinning carbon nanofibers hybrid carbon nanotubes composite anode. *Int J Hydrogen Energy*. 2019;44:3088-3098.
14. Gao Y, Yan N, Jiang C, et al. *Appl Catal B Environ*. 2020;268:118737.
15. Zhang K, Wu X, Chen J, et al. The role and related microbial processes of Mn-dependent anaerobic methane oxidation in reducing methane emissions from constructed wetland-microbial fuel cell. *J Environ Manage*. 2021;294:112935.
16. Chen S, Smith AL. Performance and microbial ecology of methane-driven microbial fuel cells at temperatures ranging from 25 to 5°C. *Water Res*. 2019;166:115036.
17. Jiang N, Huang M, Li J, et al. Enhanced bioelectricity output of microbial fuel cells via electrospinning zeolitic imidazolate framework-67/polyacrylonitrile carbon nanofiber cathode. *Biores Technol*. 2021;337:125358.
18. Das A, Kumar PM, Bhagavathiachari M, Nair RG. Hierarchical ZnO-TiO_2 nanoheterojunction: A strategy driven approach to boost the photocatalytic performance through the synergy of improved surface area and interfacial charge transport. *Appl Surf Sci*. 2020;534:147321.
19. Liang Y, Feng H, Shen D, et al. A high-performance photo-microbial desalination cell. *Electrochimica Acta*. 2016;202:197-202.
20. Sun Z, Cao R, Huang M, Chen D, Zheng W, Lin L. Effect of light irradiation on the photoelectricity performance of microbial fuel cell with a copper oxide nanowire photocathode. *J Photochem Photobiol A Chem*. 2015;300:38-43.
21. Li J, Li X, Zhao Q, et al. Polydopamine-assisted decoration of TiO_2 nanotube arrays with enzyme to construct a novel photoelectrochemical sensing platform. *Sens Actuat B Chem*. 2018;255:133-139.
22. Chen Q-Y, Liu J-S, Liu Y, Wang Y-H. Hydrogen production on TiO_2 nanorod arrays cathode coupling with bio-anode with additional electricity generation. *J Power Sources*. 2013;238:345-349.
23. Shen J, Chen D, Zhao W, Zhang Ww, Zhou H. Study on the preparation and characterizations of an improved porous Ti/TiO_2/CdS CNT/C_3N_4 photoelectrode and photoelectric catalytic degradation of methylene blue. *ChemSelect*. 2018;3:3363-3373.
24. Zhang T, Meng F, Cheng Y, Dewangan N, Ho GW, Kawi S. Z-scheme transition metal bridge of Co9S8/Cd/CdS tubular heterostructure for enhanced photocatalytic hydrogen evolution. *Appl Catal B Environ*. 2021;286:119853.
25. Cai T, Huang Y, Huang M, Xi Y, Pang D, Zhang W. Enhancing oxygen reduction reaction of supercapacitor microbial fuel cells with electrospun carbon nanofibers composite cathode. *Chem Eng J*. 2019;371:544-553.
26. Wang H, Fu B, Xi J, et al. Remediation of simulated malodorous surface water by columnar air-cathode microbial fuel cells. *Sci Total Environ*. 2019;687:287-296.
27. Yang L, Yi G, Hou Y, et al. Building electrode with three-dimensional macroporous interface from biocompatible polypyrrole and conductive graphene nanosheets to achieve highly efficient microbial electrocatalysis. *Biosens Bioelectron*. 2019;141:111444.
28. Cheng L, Zhang D, Liao Y, Li F, Zhang H, Xiang Q. Constructing functionalized plasmonic gold/titanium dioxide nanosheets with small gold

Research Article
doi.org/10.1002/ansa.202100062

nanoparticles for efficient photocatalytic hydrogen evolution. *J Colloid Interface Sci*. 2019;555:94-103.
29. Wang P, Xu S, Wang J, Liu X. *J Mater Sci Mater Electron*. 2020;31:19797-19808.
30. Yang Y, Zhang D, Xiang Q. Plasma-modified $Ti_3C_2T_x$/CdS hybrids with oxygen-containing groups for high-efficiency photocatalytic hydrogen production. *Nanoscale*. 2019;11:18797-18805.
31. Cao C, Hu C, Shen W, Wang S, Tian Y, Wang X. Synthesis and characterization of TiO_2/CdS core shell nanorod arrays and their photoelectrochemical property. *J Alloys Comp*. 2012;523:139-145.

How to cite this article: Ma J, An Z, Zhang W, Shen J, Qi Y, Chen D. TiO_2/CdS composite photocathode improves the performance and degradation of wastewater in microbial fuel cells. *Anal Sci Adv*. 2022;3:188-197.
https://doi.org/10.1002/ansa.202100062